Metallophysics and Advanced Technologies
Металофіз. новітні технол.
Metallofiz. Noveishie Tekhnol.
2025, vol. 47, No. 8, pp. 875–889
https://doi.org/10.15407/mfint.47.08.0875
Reprints available directly from the publisher

PACS numbers: 06.60.Vz, 61.72.Ff, 81.05.Bx, 81.05.Ni, 81.20.Ev, 81.40.-z, 81.70.-q

Ti-Based Metal-Matrix Composites Reinforced with TiC or TiB Particles Obtained by Electron-Beam 3*D* Printing Using a Cored Wire

D. V. Kovalchuk[*,**], V. I. Nevmerzhytsky[*,**], V. P. Tkachuk[*,**], S. V. Akhonin[***], S. L. Schwab[***], D. G. Savvakin[*], D. V. Vedel[*,****], O. O. Stasiuk[*], D. V. Oryshych[*], and P. E. Markovsky[*]

[*]*G. V. Kurdyumov Institute for Metal Physics, N.A.S. of Ukraine, 36 Academician Vernadsky Blvd., UA-03142 Kyiv, Ukraine*
[**]*JSC 'NVO Chervona Hvylia', 28 Dubrovytska Str., UA-04114 Kyiv, Ukraine*
[***]*E. O. Paton Electric Welding Institute, N.A.S. of Ukraine, 11 Kazymyr Malevych Str., UA-03150 Kyiv, Ukraine*
[****]*I. M. Frantsevich Institute for Problems in Materials Science, N.A.S. of Ukraine, 3 Omeljan Pritsak Str., UA-03142 Kyiv, Ukraine*

A metal-matrix composites (MMCs) based on titanium matrix reinforced with the TiB and TiC particles are obtained by printing with electron-beam melting and cored wires as feeding deposited material. These wires of three types are made of a mixture of fine powders of pure Ti with fine powders of (1) TiC, (2) TiB_2, or (3) Ti/TiB (obtained by preliminary sintering) wrapped into 100 μm-thick titanium foil. MMCs are formed due to the *in situ* reaction between Ti and fine hard particles during the deposition on the surface of the

Corresponding author: Oleksandr Oleksandrovych Stasiuk
E-mail: olek.stasiuk@gmail.com

Citation: D. V. Kovalchuk, V. I. Nevmerzhytsky, V. P. Tkachuk, S. V. Akhonin, S. L. Schwab, D. G. Savvakin, D. V. Vedel, O. O. Stasiuk, D. V. Oryshych, and P. E. Markovsky, Ti-Based Metal-Matrix Composites Reinforced with TiC or TiB Particles Obtained by Electron-Beam 3*D* Printing Using a Cored Wire, *Metallofiz. Noveishie Tekhnol.*, **47**, No. 8: 875–889 (2025). DOI: 10.15407/mfint.47.08.0875

base Ti–6Al–4V plate. Upon printing, the gradients in both the composition and the microstructure state of the MMCs are formed. The bottom layer adjacent to the base Ti–6Al–4V plate has relatively-low concentrations of the TiC or TiB particles, while approaching the top surface, the concentration of hardening particles increases. This gradient microstructure ensures a smooth change in hardness along the height of the MMC layer, and its maximum reaches 525–540 *HV* in the cases of wires (1) and (2), while for wire (3), which has most uniform distribution of finest strengthening particles, it is up to 640 *HV*.

Key words: titanium-matrix composite, printing with electron beam, cored wire, interphase interaction, microstructure, phase composition, titanium carbide, titanium boride.

Металоматричні композити (ММК) на основі титанової матриці, зміцненої частинками TiB і TiC, було одержано шляхом 3*D*-друку електронно-променевим методом із використанням порошкового дроту в якості матеріялу, що натоплювався. Дроти трьох типів було виготовлено із суміші дрібних порошків чистого Ti та порошків (1) TiC, (2) TiB_2 або (3) суміші Ti/TiB (одержаної попереднім спіканням), загорнутих у титанову фолію товщиною у 100 мкм. ММК утворився внаслідок реакції безпосередньо в процесі топлення між Ti та цими частинками під час осадження на поверхню базової пластини зі стопу Ti–6Al–4V. Під час 3*D*-друку утворилися ґрадієнти у фазовому складі та мікроструктурі ММК. Нижній шар, що безпосередньо прилягає до базової пластини Ti–6Al–4V, має відносно низькі концентрації частинок TiC або TiB, а, наближаючись до поверхні композиту, концентрації цих зміцнювальних частинок збільшуються. Така ґрадієнтна мікроструктура забезпечує плавну зміну твердости по висоті шару ММК, і її максимум сягає 525–540 *HV* у випадках дротів (1) і (2), а для дроту (3), який має найбільш рівномірний розподіл найдрібніших зміцнювальних частинок, сягає 640 *HV*.

Ключові слова: титановий матричний композит, 3*D*-друк електронним променем, порошковий дріт, міжфазова взаємодія, мікроструктура, фазовий склад, карбід Титану, борид Титану.

(Received 11 March, 2025; in final version, 2 July, 2025)

1. INTRODUCTION

Titanium alloys possess excellent strength-to-weight ratios and corrosion resistance. These characteristics promote their wide use in aerospace, marine and automotive industries [1–3]. However, such drawbacks of titanium alloys as insufficient hardness and wear resistance as well as increased manufacturing costs restrict their application. Hardness, wear resistance and strength level can be improved with creation of metal-matrix composites (MMCs) on the base of titanium matrixes reinforced with disperse high-moduli particles. It is general-

ly known, phases such as titanium carbide TiC and titanium monoboride TiB are the best suitable for reinforcing both commercially-pure (CP-Ti) titanium and alloyed titanium matrixes. On another hand, such characteristics of MMCs are reasons for their poor workability, creating problems with manufacturing net-shape products. Printing, also known as additive manufacturing (AM) [1, 2], is suitable approach for easy and fast manufacturing net-shape products in cost-efficient manner. printing has been widely used in industry for a long time for stainless steel and nickel-based products. However, AM technologies are less developed for titanium-based products, because of achievement of their desirable mechanical characteristics is rather problematic due to necessity for careful protection of titanium from contamination and strong microstructure control during printing process.

A promising AM technology for titanium-based products is xBeam metal-printing process [3, 4] using hollow electron beam and wire as feedstock material. Unique profile of electron-beam brings' advantages to control effectively heated area, molten pool, cooling conditions, and microstructure of crystallized metal. The noted technology was successfully used for printing various titanium-alloy products using wires of corresponding compositions. However, hard and brittle MMCs are not suitable to produce corresponding wires in conventional manner. As an alternative method to produce wires of desirable composition, so-called 'cored wire' consisted of powder mixtures sealed inside ductile foil shell, can be used [5–7]. This method is promising to obtain cored wires corresponding to titanium-based MMCs with various reinforcing additions and, then, to use noted cored wires as feedstock materials in xBeam 3*D*-printing process for MMCs' products [5, 8]. However, potential and peculiarities of xBeam 3*D*-printing process for manufacturing titanium-based MMCs reinforced with the TiC and TiB phases should be studied.

The aim of the present study is to establish the potential for using cored wires as feedstock materials for printing of MMCs, as well as peculiarities of microstructure and phase composition of 3*D*-printed products, as an example, using MMCs on the base of CP-Ti matrix reinforced with the TiC and TiB phases.

2. MATERIALS, TECHNOLOGICAL APPROACH, AND EXPERIMENTAL PROCEDURE

Two MMCs' compositions on the base of unalloyed titanium (CP-Ti) matrix reinforced with either 40% (vol.) TiC or 40% TiB were selected for present investigation. To produce the cored wires of noted compositions, titanium foil (20 μm thickness), titanium powder (40–125 μm in size), TiC (less than 30 μm) and TiB_2 (less than 10 μm) powders were used as raw materials. The cored wire manufacturing process was de-

scribed in details elsewhere [5–7]. The powders were blended in corresponding ratios and sealed in titanium foil shell 3 mm in diameter. Necessary amount of TiC powder was taken for Ti–40% TiC cored wire manufacturing, while raw TiB_2 powder was tested in two approaches to produce cored wires corresponding to 40% TiB reinforcements. First approach assumes *in situ* $TiB_2 + Ti \rightarrow TiB$ exothermic reaction to form monoboride TiB phase during printing. Second approach was comparatively used to clarify possible influence of noted reaction and heat release on microstructure formation. For the second one, the necessary amount of boron was introduced as composite Ti/TiB powder obtained with preliminary reaction sintering of $Ti + TiB_2$ powder blend at 1200°C, 1 hour in vacuum. Therefore, raw TiB_2 powder was transformed into porous Ti/TiB reaction product, which was crushed into powder again; composite Ti/TiB powder was sealed in Ti foil for manufacturing second cored wire of Ti–40% TiB composition.

The cored wires were used in the xBeam metal-printing method to print MMC products on the surface of Ti–6Al–4V (wt.%) plate as substrate. A profile electron beam in the form of a hollow inverted cone melts a cored wire that is fed coaxially with this electron beam. The advanced technological features [9–11] provided by the presented heating configuration and the use of a low-voltage (< 20 kV) but high-power (up to 18 kW) electron beam creates a moderate concentration of energy on the heating surface (in the range of 10^3 kW/cm^2), providing a number of exceptional technological possibilities for manufacturing of high-quality printed products with high productivity.

MMCs' samples of ≅ 20 mm in height and 7–10 mm in width (Fig. 1) were printed layer by layer on Ti–6Al–4V substrate using above described approach. The samples were cut with spark erosion; their verti-

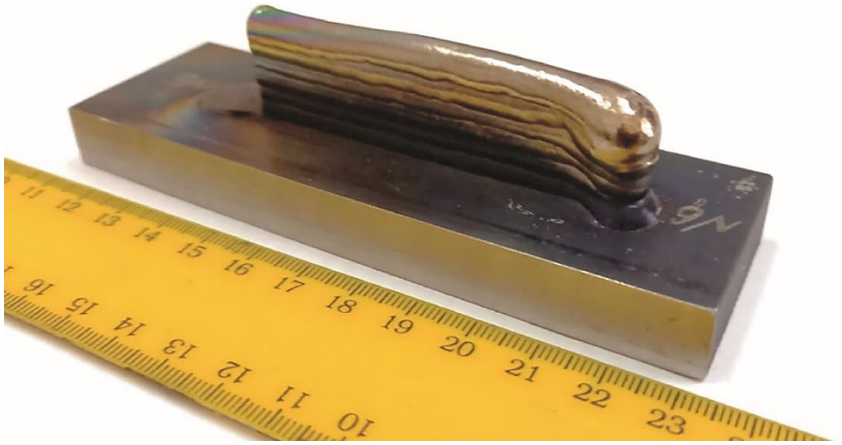

Fig. 1. General view of 3*D*-printed MMC sample.

cal cross sections were polished and etched with Kroll's reagent (2% HF, 5% HNO_3, 93% H_2O) for microstructure investigations over the sample height. Microstructure studies were performed using SEM (Tescan Vega III equipped with Brucker EDX analyser). Phase composition of materials, including transformation of boride phases, was studied with x-ray diffraction analysis. Hardness tests (Wolpert 432 SWD) were implemented to evaluate mechanical characteristics of printed MMCs.

3. RESULTS

3.1. MMCs with TiC Reinforcements

The typical microstructure of 3*D*-printed Ti–40% TiC MMC is shown in Fig. 2. The CP-Ti matrix demonstrates fine lamellar microstructure with rather miscellaneous distribution of reinforcing phase along the

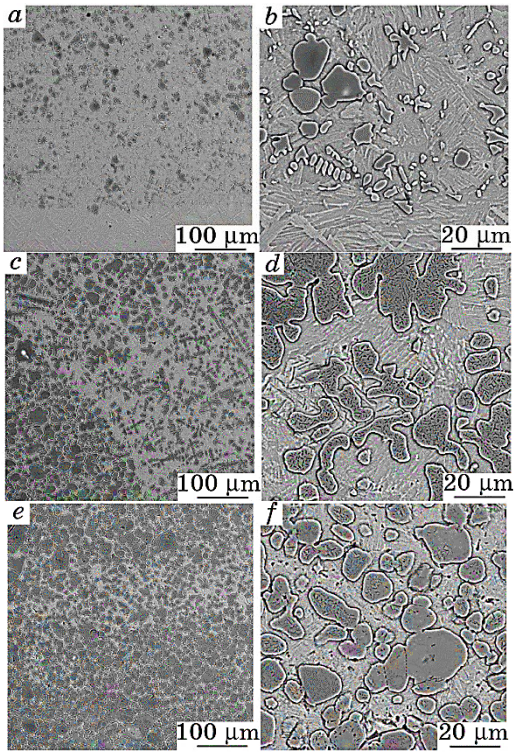

Fig. 2. Microstructure of 3*D*-printed MMC strengthened with TiC in various zones: bottom area near Ti–6Al–4V plate (*a*, *b*), the middle part (*c*, *d*), and on the top of the MMC layer (*e*, *f*) (SEM, BSE).

height of printed MMC. Bottom part of MMC adjacent to Ti–6Al–4V substrate (Fig. 2, *a*, *b*) is characterized with relatively low amount of reinforcing particles of nearly globular and needle-like/dendrite-like morphologies. Coarse globular particles (up to ≅ 25 μm in size) looks like raw TiC powder, which does not noticeably changed on 3*D*-printing process. Needle- or dendrite-like finer (1–10 μm) particles, obviously, precipitate during melting/crystallization cycles. The interface between substrate and printed MMC is sharply recognized owing to appearance and absence of reinforcing particles.

The middle part of printed MMC (Fig. 2, *c*, *d*) demonstrates quite higher amount of reinforcing particles of noticeably coarser sizes (up to 40–50 μm), their morphologies are nearly globular and dendrite-like ones.

The top part of 3*D*-printed MMC (Fig. 2, *e*, *f*) is characterized with highest observed amount of reinforcing particles up to 50 μm in size. The particles morphology is changed for mainly globular one and the average size (of about 20–30 μm) is increased due to disappearing of finer particles.

The x-ray analysis (Fig. 3) was comparatively performed for upper and bottom parts of 3*D*-printed MMC. In both locations, MMC demonstrated two-phase composition: CP-Ti matrix with α (h.c.p.) crystal lattice and titanium carbide TiC (cubic lattice) reinforced phase. At the same time, x-ray analysis confirmed obvious increase in the amount of TiC phase for upper area of MMC compared to bottom part, where diffraction peaks of β (b.c.c.) phase were also observed due to partial x-ray

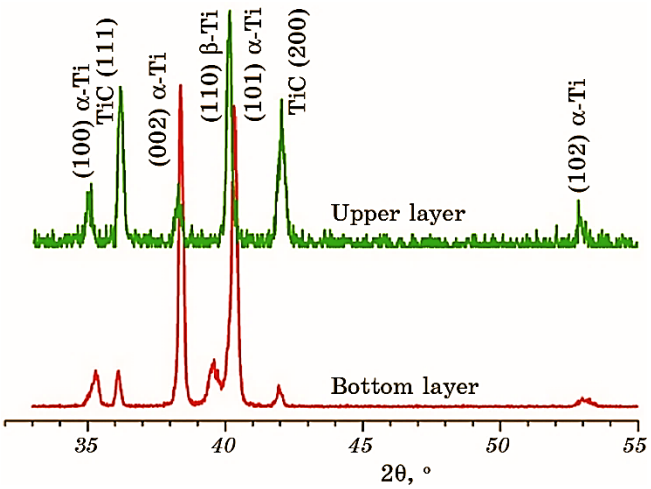

Fig. 3. Comparison of x-ray diffraction patterns for upper and bottom (near Ti–6Al–4V substrate) MMC material 3*D*-printed with a cored wire contained Ti + 40% TiC.

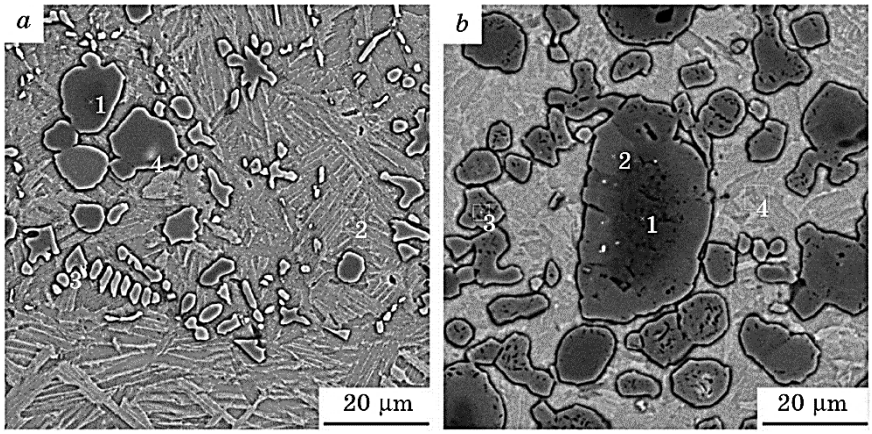

Fig. 4. Locations of the points, where chemical composition of Ti–40% TiC MMC was analysed: MMC zone near Ti–6Al–4V substrate (*a*), the middle part of printed MMC (*b*).

diffraction from Ti–6Al–4V substrate.

Local EDX analysis of reinforcing particles (Fig. 4, Table 1) revealed the main rules of carbon redistribution over the printed MMC microstructures. The composition of reinforcing particles is close to TiC titanium carbide phase, however, with some deficit of carbon content. The highest carbon content (29–33 at.%) was measured for the centre of coarse particles which allow to identify their composition corresponding to two-phase α-Ti + TiC area in Ti–C binary phase diagram [12] and stoichiometry as Ti_2C. Carbon content is obviously reduced at

TABLE 1. Local chemical composition of Ti–40% TiC MMC microstructure.

No. point	Content of chemical elements, wt.%/at.%				
	Ti	C	Al	V	W
Bottom (Fig. 4, *a*)					
1	90.70/70.98	9.30/29.02	–	–	–
2	92.61/87.30	0.88/3.29	4.61/7.72	1.90/1.69	–
3	92.69/76.91	6.72/22.22	0.59/0.87	–	–
4	82.62/70.72	7.96/27.17	0.01/0.02	–	9.40/2.10
Middle (Fig. 4, *b*)					
1	88.88/66.72	11.12/33.28	–	–	–
2	93.14/77.30	6.86/22.70	–	–	–
3	93.34/78.46	6.24/20.90	0.42/0.63	–	–
4	96.18/91.73	0.96/3.66	2.56/4.34	0.30/0.27	–

the edges of coarse particles and for fine particles (20–27%), while its measured content is minor (≅ 3%) for CP-Ti matrix.

Some penetration of Al and V from Ti–6Al–4V substrate into printed MMC matrix was observed near the interface between them (Fig. 4, *a*, Table 1, point No. 4), while traces of these alloying elements can be observed even in middle part of printed MMC (Fig. 4, *b*, Table 1, point No. 4). In addition, W impurity was observed in some TiC particles (Table 1) as result of TiC powder manufacturing process.

In accordance with microstructure changes, namely, with increase in observed amount of titanium carbide particles in CP-Ti matrix, the hardness is increased from bottom to the top parts of printed Ti–40% TiC MMC. For the area around the MMC/Ti–6Al–4V substrate interface, the hardness was within 355–396 *HV*. The hardness is increased to 438–506 *HV* for the bottom part of MMC, while it was within 409–634 *HV* at the top part of MMC.

3.2. Ti–40% TiB MMC Manufactured Using Raw TiB_2 Powder

The x-ray diffraction patterns and microstructure of Ti–40% TiB MMC printed using a cored wire with raw TiB_2 powder additions are shown in Figs. 5, 6. It should be noted, remnants of raw TiB_2 phase was not detected by x-ray analysis (Fig. 5) suggesting $Ti + TiB_2 \rightarrow TiB$ reaction was completed or, at least, nearly completed on 3*D*-printing process. Diffraction peaks of α (h.c.p.) titanium matrix and reinforcing

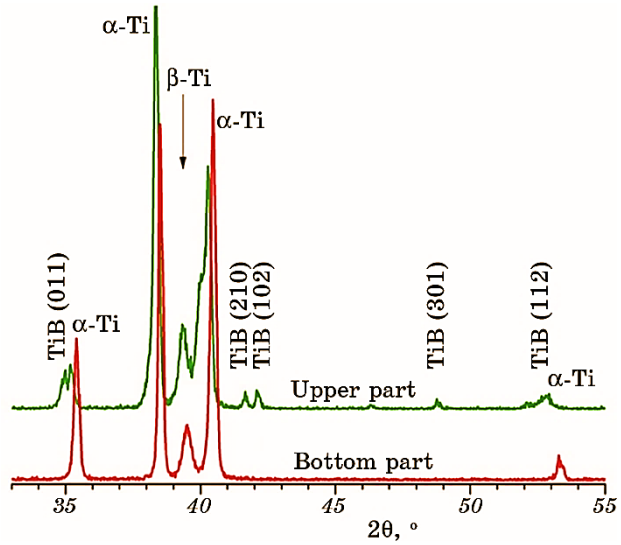

Fig. 5. Comparison of x-ray diffraction patterns for upper and bottom parts of MMC material 3*D*-printed with a cored wire containing Ti + 40% TiB_2.

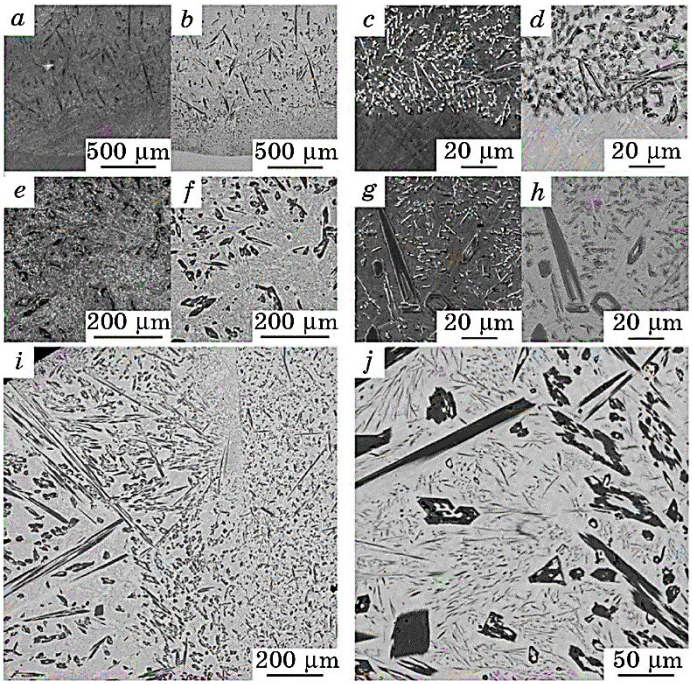

Fig. 6. Microstructure of 3*D*-printed MMC strengthened with TiB in zones: near base Ti–6Al–4V plate (*a*–*d*), in the middle (*e*–*h*), and on the top of the layer (*i*, *j*), SE mode (*a*, *c*, *e*, *g*), BSE (*b*, *d*, *f*, *h*, *i*, *j*).

TiB monoboride phase were observed with obvious tendency for increase of TiB-phase amount for upper part of MMC. In addition, traces of β-b.c.c. titanium phase were observed at x-ray diffraction patterns for bottom part of MMC due to presence of vanadium in Ti–6Al–4V substrate. Printed MMC demonstrates lamellar microstructure of titanium matrix with reinforcing precipitations having not-uniform morphology and size over the height of MMC (Fig. 6). The bottom part of MMC (Fig. 6, *a*, *b*) is characterized with relatively fine (width of 1–10 μm) needle-like precipitations of titanium boride phase, while interface between MMC and Ti–6Al–4V substrate demonstrates smallest (1–4 μm) boride precipitations. Sharp MMC/Ti–6Al–4V interface is observed on microstructure images.

For middle part of MMC (Fig. 6, *c*, *d*), the fine boride particles coexist with coarse boride precipitations up to 20 μm in width and up to 100–150 μm in length, which cross section looks like hollow hexagon shape. The distribution of coarse and fine precipitations in CP-Ti matrix is rather not uniform: near the coarse boride precipitations, matrix is free of fine ones (Fig. 6, *d*).

Upper part of MMC contains boride precipitations of wide size

TABLE 2. Chemical composition of the MMC in the different locations.

No.	Content of chemical elements, wt.% /at.%		
	Ti	B	Al
	Near the Ti–6Al–4V substrate, overall		
1	94.57/83.31	3.51/13.69	1.92/3.00
	Upper part, overall		
2	95.90/85.41	3.43/13.53	0.67/1.06

range: the coarsest boride needles (up to 1 mm in length, 50 μm width) exist together with fine precipitations between them (Fig. 6, *e*, *f*).

Despite observed microstructure non-uniformity, the total content of boron in Ti matrix measured with EDX method is slightly increased for upper part of MMC compared to bottom part (Table 2). Some aluminium additions were observed in bottom part or MMC obviously, due to penetration of this element from substrate, while the traces of this element as impurity were detected in upper part.

The hardness was changed over the height of the MMC. The lowest hardness within 399–406 *HV* was observed at the boundary with Ti–6Al–4V substrate; values of 432–447 *HV* were measured at the bottom part. The highest and variable within the wide-range hardness values were measured for top part of MMC: 430–541 *HV*.

3.3. MMC Produced Using Pre-Sintered Ti and TiB_2 Powders

Figures 7 and 8 show x-ray diffraction patterns and microstructure of MMC, which was 3*D*-printed using a cored wire produced with preliminary sintered $Ti + TiB_2$ powder blend. Similarly to previous sample, diffraction peaks corresponding to α-Ti (h.c.p.) and TiB phases were observed (Fig. 7), while traces of β-Ti (b.c.c.) were presented for bottom part of 3*D*-printed MMC. It should be noted, no obvious difference in TiB phase amount for upper and bottom parts of MMC was observed in present case.

Titanium matrix demonstrates lamellar microstructure (Fig. 8) similar to microstructure of previously described matrixes (Figs. 2 and 6) with variable size of boride reinforcements inside. However, size of boride precipitations in present case looks like more uniform than for previously described microstructure (Fig. 6), where TiB_2 powder was used without preliminary sintering. Bottom part of MMC (Fig. 8, *a*, *d*) is characterized with sharply designated MMC/substrate interface and mixture of relatively uniform near globular and needle-like boride precipitations which size is 1–10 μm in cross-sections, while length is up to 100 μm.

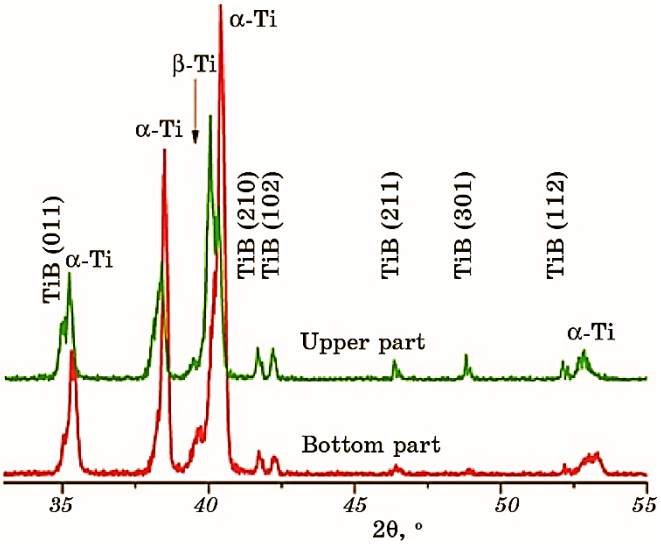

Fig. 7. X-ray diffraction patterns for lower and upper parts of MMC 3*D*-printed using a cored wire with Ti/TiB powder (as a product of preliminary sintered Ti + TiB_2 powder blend).

Central part of MMC demonstrates mainly thin and uniform needle-like boride reinforcements (Fig. 8, *c*, *f*) with higher length to width as-

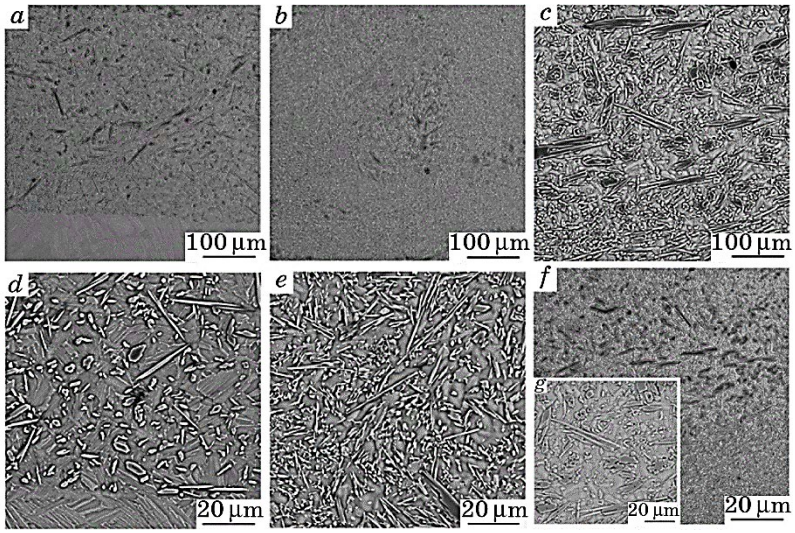

Fig. 8. Microstructure of 3*D*-printed MMC produced with pre-sintering Ti and TiB_2 powders: zone near Ti–6Al–4V substrate (*a*, *d*), the middle part of MMC (*b*, *e*), and on the top part of MMC (*c*, *f*, *g*) (SEM).

pect ratios as well as some occasional coarse laths. The coarsest borides are observed in upper part of MMC (Fig. 8, *c*, *g*, *f*), where significant amount of large laths (up to 100 μm in length and up to 20 μm in width) having hollow hexagon cross-sections co-exists with fine (of 1–5 μm) needle-like and nearly globular precipitations.

Hardness gradually increases from bottom to top of 3*D*-printed MMC; simultaneously, wider variations for measured hardness values were observed within the same area. Interface between MMC and Ti–6Al–4V substrate possesses hardness of 412–422 *HV*, bottom part of MMC demonstrates hardness within the 482–525 *HV* range, while top part of MMC was characterized with highest average hardness and widest deviation range of measured values: 532–623 *HV*.

4. DISCUSSION

Above-described results prove that desirable phase composition of 3*D*-printed MMC was achieved in all cases independently on what type of reinforcing powders (TiC, TiB_2 or Ti/TiB) was used in cored wires. At the same time, all 3*D*-printed MMCs are characterized with more or less pronounced microstructure inhomogeneity along the height of 3*D*-printed samples. This inhomogeneity is related to local amount, sizes and morphologies of reinforcing phase constituents, which, in turn, depend on powder used in cored wires and peculiarities of transformations upon 3*D*-printing process. In addition, some composition and microstructural features observed exclusively for bottom or upper part of printed MMCs are caused with specific conditions for first (bottom) and last (top) 3*D*-printed layers.

For Ti–40% TiC MMC, obvious redistribution of carbon from raw TiC powder particles during 3*D*-printing process is observed. Microstructure features shown in Figs. 2 and 4, namely, presence of dendritic-type carbide precipitations allows to suggest processes realized during printing. Titanium melting point (1668°C) is quite lower than TiC melting point (3067°C); thus, the pool locally formed during printing should consist of molten titanium and solid TiC particles. Decrease in carbon content at the edges of initial TiC particles (Fig. 4, Table 1) suggests diffusion penetration of carbon into titanium molten pool and formation of liquid Ti–C solution with gradual dissolution of TiC particle surface. Further crystallization resulted in newly formed fine dendritic-like carbide precipitations together with coarser initial TiC powder particles, while minor C content was detected in Ti matrix (Fig. 4, Table 1). Obvious increase in volume content of carbide precipitations (Figs. 2 and 3) for upper part of MMC allow to suppose delamination of components within the molten pool and upward movement of lighter, carbon-rich components on layer-by-layer melting and crystallization. Melting of Ti–6Al–4V substrate surface should take place on

printing of first MMC layers, which results in intensive mixing of liquids in molten area and penetration of alloying elements Al and V into bottom part of MMC. Saturation of bottom part of MMC with β-stabilizing element vanadium is a reason for appearance of β-phase traces (Figs. 3, 5, 7). However, with increase in height of 3*D*-printed material (*i.e.*, middle or even top parts of MMC) the concentration of aluminium and vanadium markedly reduces (Table 1).

Uneven redistribution of titanium carbide reinforcements within the Ti–40% TiC MMC microstructure is a reason for hardness variation within the wide range, this negative phenomenon is especially manifest itself for upper part of MMC (409–634 *HV*).

Contrary to MMC reinforced with TiC phase, for which started TiC powder particles preserve to a large extent and co-exist with newly formed titanium carbide dendrites, formation of MMC reinforced with TiB phase implies completed transformation of initial TiB_2 powder particles into TiB needles owing to boron diffusion through titanium matrix. The *in situ* realization of exothermic reaction between Ti and raw TiB_2 powder is an important peculiarity of Ti–40% TiB MMC manufacturing. Heat release due to reaction promotes faster boron transfer through titanium and uniform distribution of newly formed TiB needles. On the other hand, extensive heat release can result in overheating of molten pool and, hence, hardly controlled influence on microstructure of 3*D*-printed products. Thus, comparatively using cored wires with TiB_2 powder and with preliminary sintered Ti/TiB powders for manufacturing Ti–40% TiB MMCs allowed determining the better method for boron introduction in 3*D*-printing process.

Boron introduction as raw TiB_2 powder resulted in not uniform microstructure (Fig. 6) over the 3*D*-printed Ti–40% TiB MMC with increase in TiB phase content for upper part (Fig. 5). Similarly to MMC reinforced with TiC, this result also can be explained with delamination of liquid components within the molten pool and moving upward lighter boron-reached components. Slight diffraction peak of β-phase unexpectedly observed for upper part of printed MMC (Fig. 5) can be explained with some content of vanadium penetrated from substrate and presence of other β-stabilizing impurities (Fe, W, Cr) usually observed in TiB_2 and TiC powders. Another peculiarity of uneven microstructure, namely, finest TiB precipitations observed in bottom part of MMC (Fig. 6, *a*, *b*) and coarsest ones observed for top part (Fig. 6, *e*, *f*) is caused with specific (multiple cyclic) heating and cooling conditions for first printed MMC layer and last printed layer. First (bottom) printed layer adjacent to cold Ti–6Al–4V substrate is characterized with fastest cooling rates, resulting in smallest TiB precipitations. Contrary, the last (top) printed MMC layer is exposed for relatively long time at high temperatures and cooled relatively slowly due to final pass of electron beam used for smoothing of top printed surfaces. Such

heating/cooling conditions led to formation of mixture of coarse and fine TiB precipitations. Significant difference in size and morphology of observed TiB reinforcements, namely, alternation of large laths and dispersed needles in microstructure is a reason for wide variation of measured hardness values (430–541 *HV*). The relatively low and variable hardness caused with formation of phase and structural inhomogeneities, as well as possible formation of such defects of 3*D*-printing process as voids and pores, which, in turn, caused by uncontrolled kinetic and heat release of reaction between TiB_2 powder and Ti (powder and foil). Usually, this reaction started in solid state at temperatures above 900°C, however, higher temperatures and melting of titanium components in our case, obviously, significantly accelerates this reaction.

Improved microstructure uniformity of Ti–40% TiB MMC was achieved with boron introduction as Ti/TiB powdered reaction product (Fig. 8). The even microstructure was observed for almost the entire height of the printed MMC, excluding upper part, which was distinguished by above described special thermal conditions on finishing 3*D*-printing process. Moreover, contrary to both above described MMCs, x-ray analysis does not reveal noticeable difference in phase composition for bottom and upper parts of 3*D*-printed material (Fig. 7).

In this case, microstructure of Ti–40% TiB MMC is more uniform and fine in the terms of TiB sizes and its distribution inside the Ti matrix. Owing this fact, the highest level of hardness was achieved for the top part (up to 623 *HV*), while relatively-uniform hardness was achieved for bottom part (482–525 *HV*). However, decrease in hardness for bottom part of MMC is still observed, confirming preservation of some microstructural inhomogeneity even for this case. This result requires further adjustment of 3*D*-printing regimes and parameters for cored-wire manufacturing, including size of raw powders.

5. CONCLUSION

1. Ti–40% TiC and Ti–40% TiB metal-matrix composites were 3*D*-printed using profile electron beam and cored wires of corresponding compositions as feedstocks.
2. Desirable phase composition of printed MMC products was achieved in all cases, while some microstructure inhomogeneity related to higher content of reinforcing TiC and TiB phases and their larger size observed for upper part of printed MMC. In general, the possible reasons for such inhomogeneity are delamination of melt components within the molten pool and upward movement of lighter, carbon-rich and boron-rich components on layer-by-layer building of samples, as well as specific (cyclic) heating and cooling conditions for bottom and top areas of 3*D*-printed products. For Ti–40% TiB MMC produced with raw

TiB_2 powder additional reason is exothermic reaction on $TiB_2 \rightarrow TiB$ transformation giving hardly uncontrolled influence on size of boride precipitations.

3. The preliminary sintering of $Ti + TiB_2$ powder blend forms composite Ti/TiB powder, which was effectively used in a cored wire to produce most uniform and promising microstructure of Ti–40% TiB MMC with promising hardness up to 482–623 *HV*.

This work was supported by funding from the National Academy of Sciences of Ukraine within the framework of projects 07/01-2025 and 5.7/25-F. The authors express their gratitude to Dr. O. P. Karasevska for conducting the x-ray studies.

REFERENCES

1. G. Rasiya, A. Shukla, and K. Saran, *Mater. Today: Proc.*, **47**: 19 (2021).
2. L. Zhou, J. Miller, J. Vezza, M. Mayster, M. Raffay, Q. Justice, Z. Al Tamimi, G. Hansotte, L. D. Sunkara, and J. Bernat, *Sensors*, **24**: 9 (2024).
3. O. Ivasishin and D. Kovalchuk, *Additive Manufacturing for the Aerospace Industry* (Elsevier: 2019), ch. 12.
4. D. Kovalchuk, V. Melnyk, I. Melnyk, D. Savvakin, O. Dekhtyar, O. Stasiuk, and P. Markovsky, *J. Mater. Eng. Perf.*, **30**: 5307 (2021).
5. P. E. Markovsky, D. V. Kovalchuk, S. V. Akhonin, S. L. Shwab, D. G. Savvakin, O. O. Stasiuk, D. V. Oryshych, D. V. Vedel, M. A. Skoryk, and V. P. Tkachuk, *Progress in Physics of Metals*, **24**, No. 4: 715 (2023).
6. S. Schwab, R. Selin, and M. Voron, *Welding in the World*, **67**: 981 (2023).
7. S. Akhonin, V. Nesterenkov, V. Pashynskyi, V. Matviichuk, S. Motrunich, V. Berezos, and I. Klochkov, *Eastern-European J. Enterprise Technol.*, **3**, No. 12: 36 (2024).
8. P. E. Markovsky, D. V. Kovalchuk, J. Janiszewski, B. Fikus, D. G. Savvakin, O. O. Stasiuk, D. V. Oryshych, M. A. Skoryk, V. I. Nevmerzhytskyi, and V. I. Bondarchuk, *Progress in Physics of Metals*, **24**, No. 4: 741 (2023).
9. D. Kovalchuk, V. Melnyk, I. Melnyk, and B. Tugai, *Elektrotechnica & Elektronica (E+E)*, **51**, Iss. 5–6: 36 (2016).
10. D. V. Kovalchuk, V. I. Melnik, I. V. Melnik, and B. A. Tugai, *Automatic Welding*, No. 12: 26 (2017).
11. D. Kovalchuk, V. Melnyk, I. Melnyk, and B. Tugai, *Elektrotechnica & Elektronica (E+E)*, **53**, Iss. 3–4: 60 (2018).
12. H. Okamoto, *J. Phase Equilibria*, **19**: 89 (1998).